Local dynamic reconstruction in digital breast tomosynthesis

Matteo Barbieri, Clément Jailin, Laurence Vancamberg, Stéphane Roux

Local dynamic reconstruction in digital breast tomosynthesis

Matteo Barbieri[⋆,†], Clément Jailin[†], Laurence Vancamberg[⋆], and Stéphane Roux[†]

[⋆]GE HealthCare, Buc, France
[†]Université Paris-Saclay, CentraleSupélec, ENS Paris-Saclay, CNRS, LMPS – Laboratoire de Mécanique Paris-Saclay, Gif-sur-Yvette, France

ABSTRACT

Description of purpose Digital Breast Tomosynthesis (DBT) is a pseudo 3D X-ray imaging technique that limits the tissue superimposition problem observed in 2D mammography. DBT is therefore on track to become a standard of care for breast cancer screening. However, patient motion during examination is relatively common and may compromise the consistency of the reconstruction problem and decrease the conspicuity of clinical features in the resulting 3D volumes. Dynamic reconstruction of motion-polluted cases is therefore essential for patient care.

Materials & Methods The reconstruction problem is enriched to include estimation and correction of patient motion in 3D. The resolution of the dynamic problem is a two-stage process alternating between a motion-corrected reconstruction based on the SIRT algorithm and a motion estimation based on the Projection-based Digital Volume Correlation (P-DVC) method. It is coupled with a multiscale coarse-to-fine procedure which allows to capture both large and fine displacements. Additionally, the dynamic reconstruction is focused on a local region to simplify the kinematic description of patient motions and limit computation time.

Results The method was applied to 63 local regions throughout 19 DBTs showcasing motion artefacts. It enabled to significantly reduce the objective function, correct motion artefacts and visualize smaller details previously blurred.

Conclusion Dynamic tomosynthesis improves the reconstruction problem consistency and image quality by enhancing the visibility of small critical clinical features. Local reconstruction around areas of interest is a feature which helps radiologists to focus on specific details while limiting the computation time.

Keywords: Digital tomosynthesis, Dynamic reconstruction, 3D motion estimation, Digital Breast Tomosynthesis, Local digital tomosynthesis

1. DESCRIPTION OF PURPOSE

Digital Breast Tomosynthesis (DBT) is a pseudo-3D X-ray imaging method which limits the tissue superimposition problem observed in standard 2D mammography, thus increasing the conspicuity of smaller structures. However, patient motion artefacts in DBT may prevent the visibility of small clinical features.[1] Since motion artefacts are subtle and hard to detect, they lead to lower screening and diagnostic performances.

In contrast to CT imaging, where *dynamic* reconstruction is a well-studied topic,[2,3] tridimensional motion correction techniques were not — to the best of our knowledge — transposed to digital tomosynthesis. In tomosynthesis, most of the existing work is focused on the thoracic area and exploits the cyclic description of the breathing of heartbeat motion to propose a correction.[4] Nevertheless, these methods require a modification of the clinical protocol, such as the use of a surrogate signal and/or additional acquisitions. A 2D/3D technique from Marchant *et al.*[5] was used to correct for motion in breast CT and was further adapted to provide a motion detection algorithm in DBT, without introducing correction strategies.[6]

To the best of our knowledge, no 3D dynamic reconstruction method has been applied to tomosynthesis. In this respect, previous work from the authors based on the Projection-based Digital Volume Correlation (P-DVC) framework lays the fundamentals for dynamic reconstruction dedicated to digital tomosynthesis with DBT as an application case.[7] It doesn't require modifications of the examination protocols and has no restriction regarding

M. B.: E-mail: matteo.barbieri@gehealthcare.com

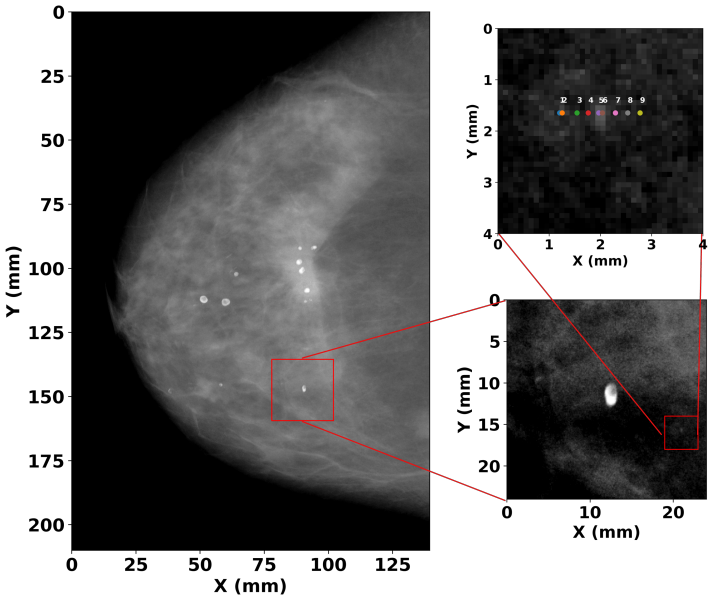

Figure 1: Visualization of a microcalcification in the 0° projection. Color points on the top right image show the x-axis translation of the object as measured on the projections.

the periodicity of the motion. Its experimental validation was performed on the BR3D CIRS phantom under plate-wise 3D Rigid Body Motion (RBMs) of significant amplitude (up to 8 mm). The study presented in this paper builds upon that result and takes the leap towards the clinical DBT application. In addition, it also extends the technique by implementing a local reconstruction to focus on a smaller volume of interest (VOI) and simplify the kinematics to estimate. In the present case, simple 3D kinematics such as a translation in the chest-nipple axis is sufficient to provide significant improvement of the image quality, while the method can easily include additional degrees of freedom when needed to correct more complex motions. Section 2 presents the available data and a brief summary of the dynamic reconstruction problem. Results on a large sample of motion-polluted cases are found in section 3 and the discussion on the benefits and drawbacks is reported in section 4.

2. MATERIAL & METHODS

2.1 Data

The approach was tested on a variety of 63 VOIs extracted from 19 different DBT cases displaying significant motion during acquisition. All DBTs were acquired during a normal breast cancer screening routine with a Senographe Pristina™ (GE HealthCare, Chicago, IL, USA) across multiple clinical facilities.

For illustrative purposes, figure 1 showcases the projection at angle 0° of a Cranio-Caudale DBT acquisition with a specific focus on the area of a macrocalcification. The higher the zooming factor, the smaller are noticeable details — such as a microcalcification on the bottom right of the initial VOI. The top right image of figure 1 aims at highlighting the presence of motion. It shows a close-up view of the microcalcification and the colored points display the relative position in the chest-nipple axis (perpendicular to the plane of motion of the source) of the detail throughout the projection series. Hence, it is clearly visible that the microcalcification (as the surrounding area) progressively shifts towards the chestwall during the acquisition process, as would be expected if a slow drift from the examined patient occurred.

2.2 Problem presentation

This study aims at solving the reconstruction problem while estimating and correcting for patient motion following the P-DVC formalism.[7] Starting from the *static* reconstruction problem, the process is based on the

minimization of the projection residuals under the assumption that the patient has nos moved during the acquisition. The projection residuals are defined as the difference between the acquired projections and the digitally computed reprojections of the reconstructed volume. With p_θ the projection data, n_{p_θ} the number of active detector pixels and Π_θ the projection operator for angle θ and $f(X)$ the reconstructed volume, the squared average norm of the projection residual is expressed as

$$r_\theta^2(f(\boldsymbol{X})) = \frac{1}{n_{p_\theta}} \|p_\theta - \Pi_\theta[f(\boldsymbol{X})]\|^2, \tag{1}$$

for angle θ and $R^2(f(\boldsymbol{X})) = \langle r_\theta^2(f(\boldsymbol{X}))\rangle_\theta$ the general projection residual metric expressed as a barycentric average of $r^2(f(\boldsymbol{X}))$ of weight n_{p_θ}/n_p. The static reconstruction problem may then be formulated as $f(\boldsymbol{X}) = \text{Argmin}_\psi\, R^2(\psi(\boldsymbol{X}))$. In the present paper, the strategy to reach the solution of this problem is algebraic and is meant to optimize data consistency.

In this respect, it is essential to ensure that all the acquired projections are taken in the same configuration of the object, which is not the case when the patient moves. To restore the consistency of the problem, additional degrees of freedom are introduced through the estimation of a displacement field $\boldsymbol{U} = \{\boldsymbol{U}_\theta\}$ describing the patient's motion at each time step. Hence, the *dynamic* reconstruction problem is expressed as

$$(f(\boldsymbol{X}), \boldsymbol{U}) = \underset{\psi, \boldsymbol{V}}{\text{Argmin}}\, R^2(\psi(\boldsymbol{X} + \boldsymbol{V}))\ , \tag{2}$$

In this case, the resolution is carried out by iterating on two sub-problems: i) a motion-corrected reconstruction from known kinematics and ii) a motion estimation from a polluted reconstructed volume. The motion-corrected reconstruction takes as an input the motion-polluted projections and the current estimate of the kinematic field and is performed using an adaptation of the trans-SIRT algorithm described by Van Eyndhoven *et al.*[8] The motion estimation is based on a linearization of the minimization problem around the current solution. By testing the sensitivity to various degrees of freedom and monitoring the projection residual, it is possible to evaluate a direction of descent and estimate an update of the kinematics for a new motion-corrected reconstruction. The search directions are defined by an N-D kinematic basis $\boldsymbol{\Phi}$ on which the global displacement field is decomposed as $\boldsymbol{U}_\theta = \sum_{j=1}^{N} u_{\theta j} \boldsymbol{\Phi}_j(\boldsymbol{X})$. Additionally, the whole process takes advantage of a pyramidal multiscale approach. At first, reconstructions are performed at a lower resolution scale and the result is passed on, after a given number of reconstruction iterations, to initiate the minimization at a higher resolution. This aims at both ensuring the validity of the linearized problem and improving computation efficiency. In this paper, the results using a single degree of freedom — a chest-nipple 3D RBM translation — are presented.

3. RESULTS

3.1 Analysis of a case with available ground truth

Figure 2 compares a *static* 2(a) and *dynamic* 2(b) reconstruction of a Cranio-Caudal (CC) DBT case. The *static* volume presents a large streaking artefact caused by the inaccurate reconstruction of the central macrocalcification. In comparison, this artefact is milder in the *dynamic* reconstruction, which speaks for a good correction of the kinematics. In addition, the bottom right microcalcification (red boxes in figure 2(b)) is significantly more conspicuous than in the *static* reconstructed volume. This is highlighted by the 4.5 mm long transversal profile averaged over 3 consecutive rows in figure 2(c), where a concentrated intensity peak is visible around 1.8 mm in the *dynamic* reconstructed image while the general intensity remains widely spread out in the profile of the static volume. This means that the consistency of the information around the specific area was restored and the reconstruction could successfully concentrate the intensity and sharpen the image. In addition, measuring the standard deviation within a small 2D bounding box including the microcalcification in the polluted and corrected volumes provides a quantitative metric of sharpness.[9] In the present example, the values are respectively $2.15 \cdot 10^{-3}$ and $3.73 \cdot 10^{-3}$ for the static and dynamic cases respectively, thus confirming that the *dynamic* reconstruction led to a sharper textured image. This suggests that the motion has been properly accounted for in the latter case.

As an additional validation, the dynamic reconstruction process provides access to the measured kinematics, which can be compared with an independent measurement. For the example of figure 2, the motion of

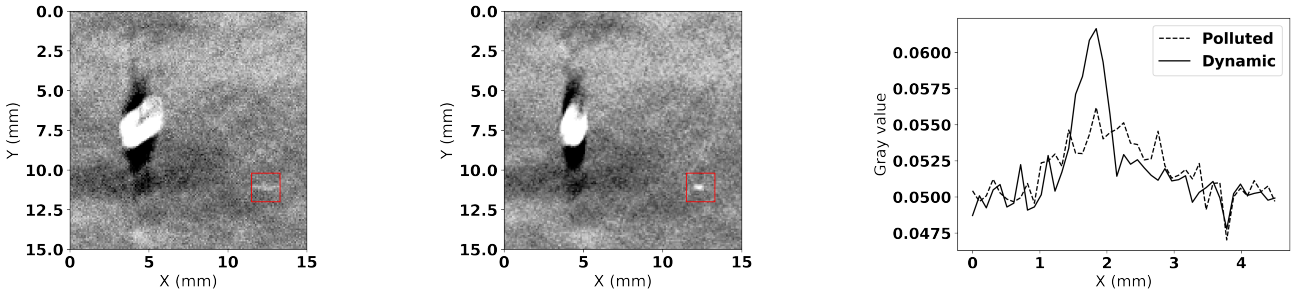

(a) Static (b) Dynamic (c) Transverse gray-level profile

Figure 2: Comparison of static (left) and dynamic (middle) reconstructions of a motion-polluted DBT case. The right figure shows a comparison of gray level profiles averaged over 3 consecutive rows across the microcalcification located in the red box

the microcalcification has been manually tracked on each radiograph, and scaled accounting for the projection magnification, to provide a reference for a quantitative comparison. Figure 3 displays the evolution of the chest-nipple translation degree of freedom for each projection angle of the dynamic reconstruction (blue), as compared to the manual measurement (dotted black). Conventionally, the position at the time of the 0° projection was taken as a reference. As can be seen from the motion estimation, over the entire sequence of acquisitions, a displacement amplitude of around 1.2 mm in the chest-nipple axis is observed, which induces a large inaccuracy in the reconstruction of textures that are less than a millimeter wide. Here, the average absolute error between both methods is shown to be 0.08 mm, which is slightly smaller than the detector pitch of 0.1 mm, (the ultimate limit of the manual tracking) and demonstrates the coherence of such techniques.

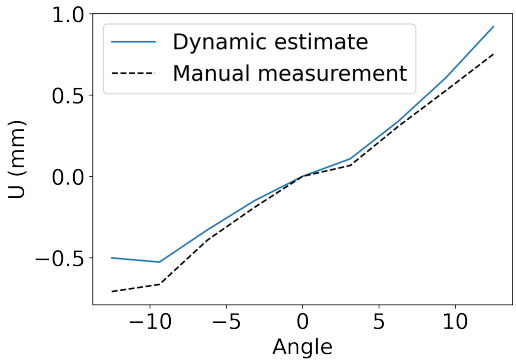

Figure 3: Comparison of two independent motion estimation for a microcalcification of figure 2: manual measurement (dotted black), dynamic motion estimate (blue)

3.2 Analysis of a larger dataset

For generalization purposes, the local dynamic reconstruction algorithm has been run on 63 VOIs extracted from 19 DBT cases. Each case was processed with a fixed number of 10 iterations per reconstruction, 5 displacement field estimations per reconstruction scale and 4 consecutive scales, namely 1:10, 1:5, 1:2 and 1:1. In total 200 reconstruction iterations and 20 displacement field estimations were performed for each VOI. *Static* and *dynamic* reconstructions have been run in parallel (*i.e.,* same scales, and same number of iterations per scale) to ensure a fair comparison.

For all 63 cases, the *static* and *dynamic* projection residuals metric R (*i.e.,* Root-Mean-Square (RMS) value) were computed and compared, which showed that 63% of the cases were improved by the dynamic process. In this respect, performing a Wilcoxon signed-rank test on the difference of the RMS asserts that the median of the *dynamic* reconstruction residuals is significantly lower than the one of the *static* reconstructions ($p < 0.05$).

For illustrative purposes, figure 4 displays a visual comparison for 5 cases — labeled (a) to (e) — based on the reconstructions as displayed for clinical evaluation. The two first columns present side by side and with the same gray level dynamics the images of 2D slices respectively obtained from *static* and *dynamic* reconstructions. The third column reports the evolution over the reconstruction iterations of the projection residual metrics $R(f(\boldsymbol{X}))$ and $R(f(\boldsymbol{X}+\boldsymbol{U}))$ respectively for both the *static* and *dynamic* reconstruction strategies. On these curves, the changes of reconstruction scale are visible every 50 iterations, where the introduction of additional details in the projections used for the reconstruction leads to a temporary increase of the metric. For the dynamic reconstruction, an update of the displacement field is performed every 10 iterations. The values of the average projection residuals typically decay until reaching a final value which was used for the previously described Wilcoxon test.

The local VOIs for all cases (a-e) were selected so that at least one calcification is apparent at the center of the reconstruction, sometimes so obvious that it produces streaking artefacts (c), sometimes quite faint (d).

- In the *static* reconstruction, cases (a), (b) and (c) present a classical effect of replication of the material point caused by motion and the resulting inconsistency between the different projections (first column of Figure 4). Correspondingly, focusing on these central calcifications, they appear as much better focused in *dynamic* reconstruction (second column of Figure 4). While on the one hand the visual results are very satisfactory, on the other hand the progress observed in the RMS displayed in the last column of Figure 4, appears as more ambiguous. For all five cases, dynamic residuals are lower than static ones, sometimes by a large amount ((a), (b), (d)), sometimes only hardly visible ((c), (e)). Nonetheless, case (c) shows a visual improvement as valuable as for cases (a) and (b) while displaying a very limited improvement in the residual norm.

- As for case (d), the central calcification is very faint and bears little weight in the projection residuals. It becomes less visible in the dynamic reconstruction while the metric significantly decreases (4d3), signaling a better consistency with the original projections. However, parts of the image (like the top left and bottom right corners) seem to be better resolved by the *dynamic* reconstruction. Hence, the simplicity of the chosen kinematic basis is not sufficient to restore the full registration of all the features of the image and trade-offs must be made, depending on the respective weights of the features in the projection residuals.

- Case (e) displays a cluster of bright calcifications which are largely polluted by motion. In addition, figure 4e1 seems to suggest that all the calcifications are not moving in the same direction since the streaks left behind the calcifications by the reconstruction are not in the same directions. The *dynamic* reconstruction does not seem to show any significant visual improvement and the reading of the residual loss is only slightly lower than the original static one.

- Finally, most of the figures 4a3, 4b3, 4c3, 4d3 and 4e3 present accidents in the evolution of $R(f(\boldsymbol{X}+\boldsymbol{U}))$ in the first 50 iterations (most visible at iteration 10 in figure 4a3). These perturbations become ever less visible as the estimation of the displacement field stabilizes. Reasons for these discontinuities include the estimation of large motions which contrast very much with the original motionless assumption. As a result, they bring in the VOI objects that were not reconstructed yet and need to be progressively integrated. For instance, this is seen in the reconstruction of case (a), which is at the limit of the chest wall. Finally, a slow convergence of the displacement field estimation that overshoots several times before stabilizing can also be observed in some cases not shown here.

4. DISCUSSION

The presented method is designed to improve tomosynthesis reconstruction of motion-polluted cases by minimizing the projection residual norm, R. The decrease was shown to be on average statistically significant and visual comparison of reconstructed volumes reports encouraging improvement of image quality. In accordance with the current hypothesis, most impressive results are achieved when the motion of the patient is in the chest-nipple axis and homogeneous across the whole VOI, like in case (a) of figure 4, where the appearance of the two calcifications are corrected by a single degree of freedom. However, improvement of the projection residual and/or reconstructed volume are not systematic. Reasons for such an apparent discrepancy are now discussed.

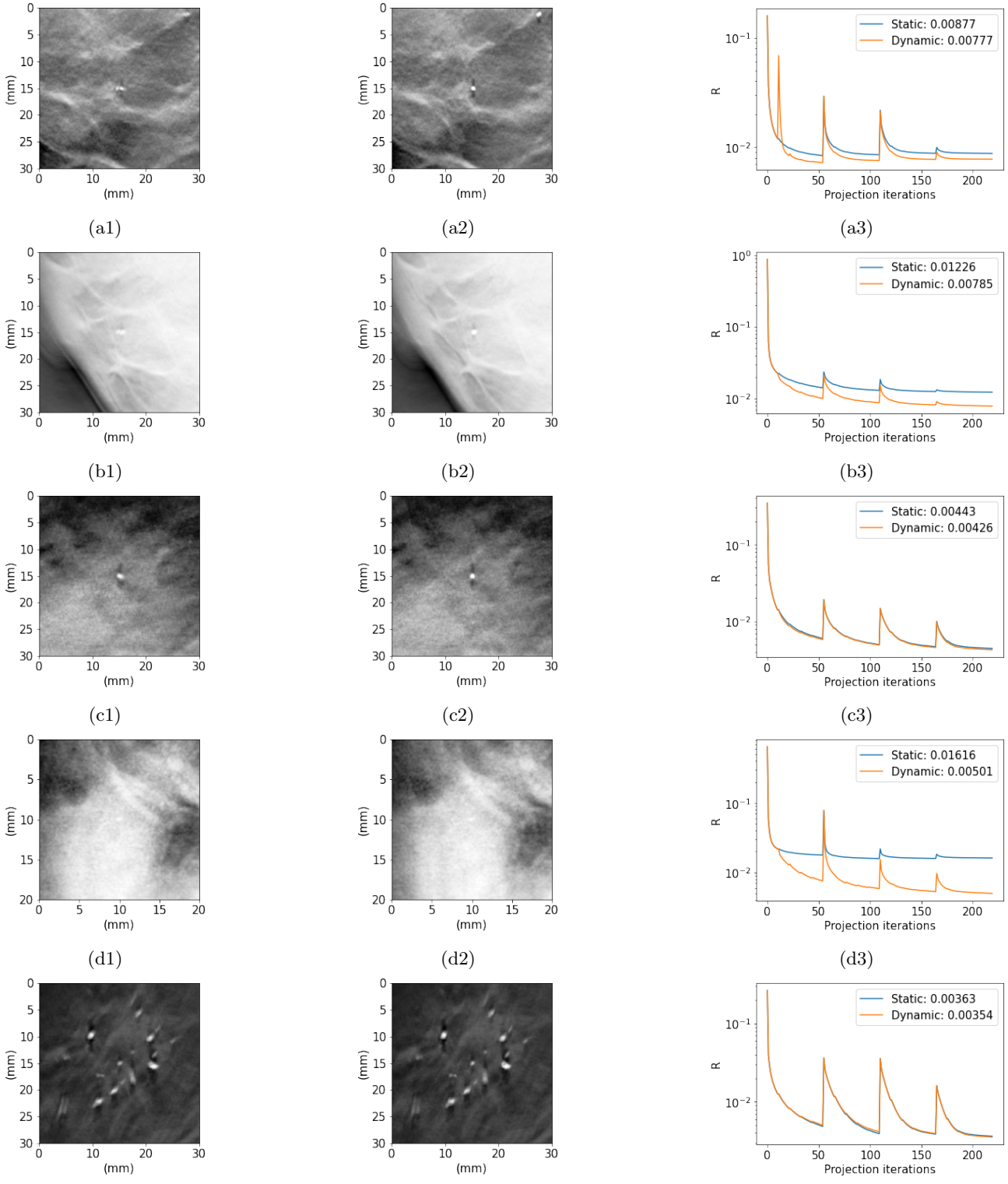

Figure 4: *Static* (left) and *dynamic* (middle) reconstructions with the same gray scale dynamics for five examples (labeled a-e). The right column displays the corresponding evolution of the average residual projections norm along iterations, (blue curve for static, orange for dynamic). Every 50 iterations, a finer resolution is considered, and for the dynamic case, the displacement is updated every 10 iterations.

In the first place, it is important to recall that tomosynthesis reconstruction is a problem based on incomplete data. So far, the present paper has focused on the advantages of a *local* reconstruction (namely simpler kinematic description and computation efficiency), however this strategy has its own limits. Since the reconstructed volume has a smaller projection area, artefacts coming from truncated projections are more pronounced. As the reconstruction requires projection rays which are attenuated by breast tissue both *inside* and *outside* of the VOI, the reconstruction of the outer part of the VOI may be significantly corrupted by the lack of information. This effect is enhanced for local tomosynthesis where the affected volume represents a larger fraction of the whole. To counter this difficulty, applying continuation strategies to the backprojected volume in order to minimize information loss from truncated projections may be explored in a further work.[10]

Secondly, the poor quality of flatfield correction leads to discrepancies in the projection residuals and has revealed to be a limiting factor. While such artefacts are also visible in *static* reconstructions, their influence on image quality is usually disregarded. However, in *dynamic* reconstruction, a spurious motion may be an opportunity to reduce the residual norm, even if not physically present. As a consequence, the estimated displacement may reach unreasonably high amplitudes in some cases without improving the visual appearance of the reconstructions. Most cases were corrected by forcing the mean of each projection residual to be null, but effort should be put into ensuring collection of the flatfields associated with each patient case.

In addition, it may be noticed that the correlation between the visual and analytical improvement is not obvious, as a large decrease in the residual does not strictly imply a large visual improvement and *vice versa*. In some cases not shown here, a visual improvement of a specific clinical feature can be observed while the residual norm of the dynamic reconstruction has increased. At variance with the discussion on a specific very local feature (section 3.1), the choice was made here to use a global indicator, the projection residual norm, which lies at the heart of the algebraic reconstruction method. This difference of weight from a single feature to a global analysis may explain the contrast in the observed gains, but it is worth underlining that even with a very modest change in the final value of residuals, the visual impression may appear very convincing for diagnosis (see *e.g.,* case (c)).

Furthermore, it is important to remember that the present paper has focused on correcting artefacts with 3D RBMs in the chest-nipple direction. Hence, only cases that display motion that can (totally or in part) be decomposed on the simplified kinematic basis may showcase visual improvement. Additionally, as the motion estimation is determined over the entire VOI, it is a compromise which may do justice to some aspects but not all, if the actual motion is poorly described by the *a priori* chosen displacement basis. This is particularly visible in case (e), where many calcifications seem polluted by motions in different directions. As a consequence, the *dynamic* reconstruction has provided a compromise which improves the projection residual but does not significantly improve the image quality of the reconstruction. This shows that even though most of the time a simple RBM may bring a significant improvement, such kinematic basis is not rich enough to entirely correct for the complex motion of the patient. Additional degrees of freedom should be integrated to account for such cases, which may be easily implemented in the proposed framework.

Finally, as for computational cost, the *dynamic* reconstruction process is more expensive than the original static version. Here, a ratio of 4 was measured between both methods. However, the computational burden depends on the size of the selected VOIs and exact number of reconstruction iterations chosen for the process. Though this estimation is expected to increase with the dimension of the kinematic basis, the mentioned total cost does not involve any optimization (*e.g.,* on the number of iterations or selecting appropriate convergence conditions). In addition, as the running of a *static* reconstruction is relatively cheap (especially in the first iterations at low resolution), a simple test of comparison with the static reference can identify early on whether the completion of the *dynamic* reconstruction is worth the time. Likewise, this can also be implemented to sort out when to display a *dynamic* reconstruction to a clinician.

5. CONCLUSION

The proposed dynamic tomosynthesis technique has been shown to achieve a significant reduction in motion artefacts in reconstructed volumes and restoring image quality. The focus on a local area reveals the kinematics in a small portion of the breast which allows to simplify the kinematic basis supporting the identification. Let us underline that, despite the above-discussed detail-oriented image quality improvements, the optimization is performed on the whole projection residual resulting from the reconstruction. In other words, the method

does not require to pinpoint interesting features to perform the dynamic reconstruction. Nevertheless, the use of existing Computed Assisted Diagnostic tools that identify areas of interest could be exploited to anticipate a local dynamic reconstruction before the radiologist wishes to examine it. In addition, multiple local reconstructions are expected to yield information that can be combined to approach a reconstruction of the whole sample even with complex dynamics. Alternatively, slightly more complex kinematic descriptions may be required to correct the motion of all the features present in the selected VOIs and will be pursued in the future.

Acknowledgement

M. B. acknowledges the support of a CIFRE Ph.D. grant from ANRT # 2021-1460, and GE HealthCare.

Compliance with Ethical Standards

This research study was conducted retrospectively using anonymized human subject data made available by research partners. All clinical data were acquired with the approval of the ethical committee. Applicable law and standards of ethic have been respected.

REFERENCES

[1] Geiser, W. R., Einstein, S. A., and Yang, W. T., "Artifacts in digital breast tomosynthesis," *American Journal of Roentgenology* **211**(4), 926–932 (2018).

[2] Wang, J. and Gu, X., "Simultaneous Motion Estimation and Image Reconstruction (SMEIR) for 4D cone-beam CT," *IEEE Nuclear Science Symposium Conference Record* **40**(10), 101912 (2013).

[3] Jailin, C., Roux, S., Sarrut, D., and Rit, S., "Projection-based dynamic tomography," *Physics in Medicine and Biology* **66**(21) (2021).

[4] Zhao, C., Herbst, M., Weber, T., Vogt, S., Ritschl, L., Kappler, S., Siewerdsen, J. H., and Zbijewski, W., "Image-domain cardiac motion compensation in multidirectional digital chest tomosynthesis," (2021).

[5] Marchant, T. E., Price, G. J., Matuszewski, B. J., and Moore, C. J., "Reduction of motion artefacts in on-board cone beam CT by warping of projection images," *British Journal of Radiology* **84**(999), 251–264 (2011).

[6] Ren, B., Zhang, Y., Ruth, C., Smith, A., Niklason, L., Tao, Z., and Jing, Z., "Automatic patient motion detection in digital breast tomosynthesis," *Medical Imaging 2011: Physics of Medical Imaging* **7961**, 79615F (2011).

[7] Barbieri, M., Jailin, C., Vancamberg, L., and Roux, S., "Dynamic tomosynthesis: A phantom proof of concept for breast care," (2024).

[8] Van Eyndhoven, G., Sijbers, J., and Batenburg, J., "Combined motion estimation and reconstruction in tomography," in [*Computer Vision – ECCV 2012. Workshops and Demonstrations*], 12–21 (2012).

[9] Batten, C. F., Holburn, D. M., Breton, B. C., and Caldwell, N. H. M., "Sharpness search algorithms for automatic focusing in the scanning electron microscope," *Scanning* **23**(2), 112–113 (2001).

[10] Kim, B., Yim, D., and Lee, S., "Development of a truncation artifact reduction method in stationary inverse-geometry x-ray laminography for non-destructive testing," *Nuclear Engineering and Technology* **53**(5), 1626–1633 (2021).